Experimental Feedback Control of Flow Induced Cavity Tones

Randolph H. Cabell*, Michael A. Kegerise†, David E. Cox‡, Gary P. Gibbs*
NASA Langley Research Center, Hampton, VA 23681

Abstract

Discrete-time, linear quadratic methods were used to design feedback controllers for reducing tones generated by flow over a cavity. The dynamics of a synthetic jet actuator mounted at the leading edge of the cavity as observed by two microphones in the cavity were modeled over a broad frequency range using state space models computed from experimental data. Variations in closed loop performance as a function of model order, control order, control bandwidth, and state estimator design were studied using a cavity in the Probe Calibration Tunnel at NASA Langley. The controller succesfully reduced the levels of multiple cavity tones at the tested flow speeds of Mach 0.275, 0.35, and 0.45. In some cases, the closed loop results were limited by excitation of sidebands of the cavity tones, or the creation of new tones at frequencies away from the cavity tones. Nonetheless, the results validate the combination of optimal control and experimentally-generated state space models, and suggest this approach may be useful for other flow control problems. The models were not able to account for non-linear dynamics, such as interactions between tones at different frequencies.

*Research Scientist, Structural Acoustics Branch, NASA Langley Research Center Mail Stop 463, Hampton, VA, 23681, randolph.h.cabell@nasa.gov, gary.p.gibbs@nasa.gov

†Research Scientist, Flow Physics and Control Branch, NASA Langley Research Center, Mail Stop 170, Hampton, VA 23681, michael.a.kegerise@nasa.gov

‡Research Scientist, Guidance and Control Branch NASA Langley Research Center, Mail Stop 170, Hampton, VA 23681, david.e.cox@nasa.gov

Nomenclature

$\mathbf{A}$	state transition matrix
$\mathbf{B}$	input matrix
$\mathbf{C}$	output matrix
$\mathbf{D}$	feedthrough matrix
J	performance function
$\mathbf{K}$	feedback gain vector
$\mathbf{I}$	identity matrix
Q	output weighting matrix
r	effort weighting
u	actuator input
v	disturbance input
$\mathbf{w}$	sensor noise vector
$\mathbf{x}$	state vector
$\mathbf{y}$	output vector
α	Rossiter phase-lag term
κ	phase speed of instability wave
$()^c$	cavity system
$()^f$	frequency system
$()_k$	value at kth sampling instant

Introduction

The generation of tones by flow over a rectangular cavity is a well known aeroacoustic phenomenon that affects landing gear and weapons bays on aircraft. Key elements of this phenomenon include instability wave growth and convection in the cavity shear layer, unsteady shear-layer impingement on the downstream cavity corner, upstream propagation of sound from the trailing-edge noise source, and conversion of sound to instability waves at the cavity's leading edge through a receptivity process. The sound pressure levels of the resulting tones can be very high, creating a noise problem inside the aircraft and possibly destroying delicate instrumentation in the cavity.

While the reduction of high sound pressure levels is important, the cavity tone problem is also a useful testbed for active flow control studies. Active flow control is of interest in application areas such as drag reduction, lift enhancement, and maneuverability for advanced vehicles[1,2] A narrow cavity in a wind tunnel is a low-dimensional testbed which retains important attributes of more complex flow problems such as limited actuator authority, nonlinearities, and a lack of physics-based models that can be used for control design. The goal of the work discussed here is to investigate and develop feedback control methodologies

for the cavity problem that will be useful for other flow-control problems.

The literature on the cavity tone problem is understandably focused on reducing the levels of the tones, rather than on using the cavity as a testbed for flow control. Nonetheless, past studies provide important insights into the physics of cavity tone generation and control, and more recent work describes sophisticated control approaches that could be applied to other flow control problems. Previous control approaches for the cavity tones can be broadly classified as being based on either passive, open loop active, or closed loop active methods. Passive approaches include rods and spoilers mounted on the leading edge of the cavity.[3] These methods can be effective for a limited range of flow conditions, but they don't provide extensive insight into the dynamics of the cavity that could be used for feedback control design.

Open loop active methods do not involve a closed feedback loop, but still provide useful information on actuators and sensors. These methods generally involve steady or unsteady blowing at the cavity's leading edge. For example, unsteady blowing can be used to drive the shear layer at a frequency different from the cavity resonance frequencies,[4–6] and thereby reduce shear layer amplification of energy at the resonance frequencies. This is a clever use of the non-linear behavior of the shear layer, but the approach offers limited information on the linear dynamics of the cavity. Alternatively, mass can be injected just upstream of the cavity's leading edge[7] in order to thicken the boundary layer and reduce the growth of instabilities in the shear layer. The optimum mass flow rate depends on the flow speed, but as with the unsteady blowing, the approach provides limited insight into the dynamics of the cavity tone problem over a large bandwidth.

Closed loop active methods which treat the cavity as a dynamical system are of particular interest for feedback flow control. Much of the early work on closed loop control of cavity tones involved manual tuning of the gain and delay of simple feedback loops at frequencies of the cavity tones.[8–13] The general approach in these previous studies was to feed the bandpass-filtered response of a microphone inside the cavity to an actuator, such as a synthetic jet or bending flap, at the leading edge of the cavity. A tunable gain and delay on the feedback signal were adjusted for maximum tone reduction. Reductions of 10-20 dB in the sound pressure level of a single tone were demonstrated, with modest additional reductions at multiple tones. These closed loop active methods were found to require an order of magnitude less energy than open loop active methods for reducing cavity tones.[9]

A desire to eliminate manual tuning of the gain and delay of the feedback loops led to the application of adaptive disturbance rejection algorithms based on low order models of an actuator and sensor system in a cavity. For example, Cattafesta applied an adaptive disturbance rejection algorithm to a subsonic compressible cavity flow,[14] where the dynam-

ics of the actuator to sensor response near a cavity tone were modeled as a second order system. The controller used an ARMARKOV adaptive disturbance rejection algorithm,[15] and achieved reductions of 10 dB on a single tone, although an actuator failure may have hindered performance. Another approach to automatically tune control parameters for a separated shear flow problem is described by King.[16] In that work, robust control methods were used to optimize the excitation frequency and amplitude for synthetic-jet actuators, positioned at the edge of a backward facing step, to manipulate the reattachment length behind the step. The dynamics of the actuator to sensor path were modeled using first or second order models plus a time delay. Robust control methods were used to create feedback controllers that compromised robust stability, disturbance rejection, and control energy.[16]

More complicated dynamical models of the cavity have also been used to generate feedback controllers for cavity tones. A linear quadratic regulator was used to control a single mode resonance at low Mach numbers (<0.15).[17] This approach is attractive because it provides a rigorous framework for controller design. Physics-based models of the tone generation mechanism in a cavity have also been proposed for control design purposes.[10,13] The model consists of a series of transfer functions, where time delays due to downstream propagation in the shear layer and acoustic propagation upstream in the cavity are important features of the model. While such a model is useful for physical insight, no such model is currently available with the accuracy needed to design and implement a feedback controller.

In contrast to earlier feedback control approaches, the current work treats control of cavity tones as a broadband feedback control problem, where the bandwidth of interest spans more than one thousand Hertz and contains multiple cavity tones. A synthetic jet was positioned at the leading edge of the cavity as a control actuator, and two dynamic pressure transducers located in the cavity were used as error sensors. A high-order state space model, generated from experimental data, was used to capture the important dynamics of the actuator-sensor system over the bandwidth of interest at a given flow speed. Discrete-time, linear quadratic control design methods, augmented with frequency shaping,[18] were used to design feedback controllers. These methods were chosen because they are well understood and can be based directly on experimentally identified models of the system being controlled. While the resulting models and controller are not explicitly derived from physics-based insights, the goal of this work was to study the suitability of experimentally based control design in flow-control applications. In addition, the approach can be readily extended to a predictive control method which integrates model identification and control design,[19] leading to a fully adaptive controller.

Feedback control tests were conducted on a cavity located in the Probe Calibration Tunnel at NASA Langley Research Center. Tests were conducted at flow speeds of Mach

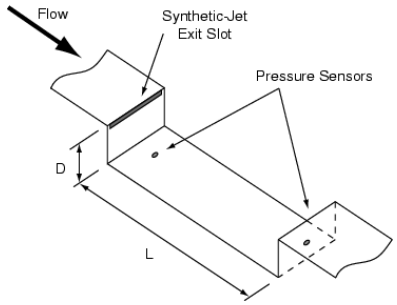

Figure 1: Schematic of cavity

0.275, 0.35, and 0.45. Over 260 control designs were tested, involving variations in model order, controller order, controller bandwidth, and estimator design.

The paper begins with a description of the system identification and control design methods. The Experimental Setup section contains descriptions of the tunnel, cavity, and control transducers. The Results section describes analysis of the test data, including the cavity response with no control, and transfer function models of the control system. Example closed loop results at each flow speed are discussed and compared with models of the closed loop transfer function. The paper ends with results which illustrate the limitations of linear models for this problem.

Analysis

The control design methodology was based on linear quadratic control methods. The approach required identification of a state space model from experimental data, design of a state estimator, and computation of the feedback gains. This section of the paper begins with a brief description of the experimental testbed, since several design choices were driven by characteristics of the testbed.

The feedback control system was used on a simple rectangular cavity with an actuator on its leading edge and pressure sensors inside the cavity. A schematic of the cavity is shown in Fig. 1. In the diagram, flow goes from upper left to lower right over the cavity. A synthetic-jet actuator was located at the cavity's leading edge, oriented so the jet's exit flow introduced disturbances parallel to the free stream direction. This design was based on the results of Williams *et al.*,[8,12] suggesting this orientation to be optimal. Pressure sensors were located in the wall below the cavity's trailing edge and in the floor of the cavity near the leading edge, as indicated in the figure.

The dynamics of the cavity were assumed to be linear and time-invariant (LTI). A block diagram of the control system applied to the cavity is shown in Fig. 2. With the LTI assumption, the cavity is represented by a transfer function relating pressure sensor responses to synthetic jet input. As shown in the diagram, an external disturbance was assumed to

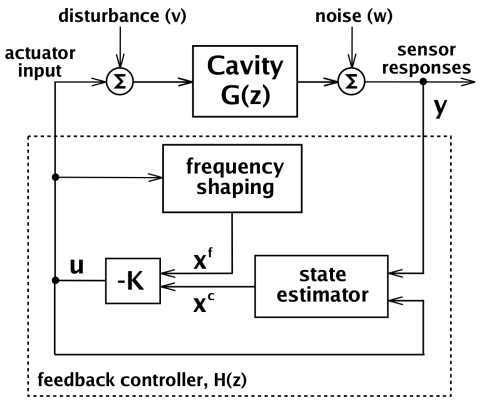

Figure 2: Block diagram of control system

enter the cavity coincident with the synthetic jet actuator, so the control designs were posed as disturbance rejection from the actuator. This assumption is not entirely accurate, but it was used because the true disturbance input is difficult to model and could not be determined from the current experimental data. The assumption provides for an appropriate general trend because active control will add damping and reduce peak responses, but precludes a direct comparison of predicted and experimental results.

A state space model was assumed for the dynamics from the actuator input to the sensor responses. This model is written

$$\begin{aligned} \mathbf{x}^c_{k+1} &= \mathbf{A}^c\mathbf{x}^c_k + \mathbf{B}^c(u_k + v_k) \\ \mathbf{y}^c_k &= \mathbf{C}^c\mathbf{x}^c_k + \mathbf{w}_k \end{aligned} \tag{1}$$

where no direct feedthrough of the inputs has been assumed.

The matrices $\mathbf{A}^c, \mathbf{B}^c, \mathbf{C}^c, \mathbf{D}^c$ were computed from experimentally measured input-output data using the eigensystem realization algorithm (ERA).[20,21] The ERA algorithm is a "black-box" identification method, so-named because the only free parameter in the model is the number of degrees of freedom. The model does not include any physics-based dynamics with tunable parameters, for example, hence the identified states are difficult to correlate with the application physics. Nonetheless, this identification approach has been useful on high order plants with complex dynamics, where a model based on first principles cannot adequately capture important aspects of the problem.[22]

In this application, the order of the state space model was chosen so the frequency responses of the identified model reproduced the spectral responses of the sensors as seen from the control actuator. High model orders, ranging from 150 to 200 states, were generally needed to obtain a model that accurately reproduced the dynamics near the cavity tones. Once the model was identified, a balanced realization truncation method [18, Ch. 10] was

used to reduce the model size to 60 states before the controller was designed. This smaller model size was needed for enabling a real-time control implementation. A further reduction in the model size would be desirable so the model parameters could be more easily related to the underlying physics of the cavity. However, minimizing the model size was not a goal of the present work.

The input-output data used to identify the model were collected by driving the synthetic jet with a broadband signal and recording the corresponding sensor responses. This procedure was done with flow present over the cavity, since the cavity dynamics are determined by the flow. The identified model was assumed to be accurate only at the single flow speed where the input-output data were collected.

To reduce control spillover and actuator saturation due to out-of-bandwidth control energy, a frequency-dependent penalty was applied to the control signal. The synthetic jet actuator had authority in a limited bandwidth containing three or four of the cavity tones, making it difficult to obtain an accurate system identification at all frequencies. To compensate for the limited actuator authority, a frequency-dependent penalty was inserted in the feedback loop to restrict control energy to the frequency range containing the cavity tones. The approach was based on augmenting the plant model in Eq. 1 with filter dynamics, $\mathbf{A}^f, \mathbf{B}^f, \mathbf{C}^f, \mathbf{D}^f$ to create an additional plant output.[18] This additional dynamical system is labeled in the block diagram in Fig 2 as the frequency shaping system. The frequency shaping was accomplished using a bandstop filter, where the magnitude of the filter corresponded to the amount of control effort penalty. Hence, the stopband contained the most significant three or four cavity tones in order to not penalize control effort in that frequency range. The passband of the filter, at frequencies above and below the cavity tones, penalized control effort in these areas. The upper and lower corner frequencies as well as the passband gain were all control design parameters. Combining the cavity and frequency shaping systems yields the single state space system

$$\begin{bmatrix} \mathbf{x}^c \\ \mathbf{x}^f \end{bmatrix}_{k+1} = \begin{bmatrix} \mathbf{A}^c & 0 \\ 0 & \mathbf{A}^f \end{bmatrix} \begin{bmatrix} \mathbf{x}^c \\ \mathbf{x}^f \end{bmatrix}_k + \begin{bmatrix} \mathbf{B}^c \\ \mathbf{B}^f \end{bmatrix} u_k + \begin{bmatrix} \mathbf{B}^c \\ \mathbf{0} \end{bmatrix} v_k \tag{2}$$

with output vector

$$\begin{aligned} \begin{bmatrix} \mathbf{y}^c \\ y^f \end{bmatrix}_k &= \begin{bmatrix} \mathbf{C}^c & 0 \\ 0 & \mathbf{C}^f \end{bmatrix} \begin{bmatrix} \mathbf{x}^c \\ \mathbf{x}^f \end{bmatrix}_k + \begin{bmatrix} \mathbf{0} \\ \mathbf{D}^f \end{bmatrix} u_k + \begin{bmatrix} \mathbf{w}_k \\ 0 \end{bmatrix} \\ \mathbf{y}_k &= \mathbf{C}\mathbf{x}_k + \mathbf{D}u_k + \begin{bmatrix} \mathbf{w}_k \\ 0 \end{bmatrix} \end{aligned} \tag{3}$$

The controllers were designed to minimize the quadratic performance function

$$\begin{aligned} J &= \sum_{k=1}^{\infty} \mathbf{y}_k^T \mathbf{Q} \mathbf{y}_k + r u_k^2 \\ &= \sum_{k=1}^{\infty} \mathbf{x}_k^T \mathbf{C}^T \mathbf{Q} \mathbf{C} \mathbf{x}_k + (\mathbf{D}^T \mathbf{Q} \mathbf{D} + r) u_k^2 \end{aligned} \tag{4}$$

where the non-negative definite matrix $\mathbf{Q}$ defines the performance of the system, and r is a positive scalar that sets a frequency-independent control effort penalty. Note that including the response of the frequency shaping system as a plant output enables the effort penalty to be applied without introducing a phase delay, as would occur with inline filtering of the actuator signal.

The optimal control corresponding to Eq. 4 is implemented as

$$u_k = -\mathbf{K} \mathbf{x}_k \tag{5}$$

A solution for the optimal controller, given the augmented plant model (Eqs. 2 and 3), $\mathbf{Q}$, and r, is well known[18] and is implemented in many engineering software packages.

A discrete Kalman estimator was used to estimate the cavity model states, $\mathbf{x}_k^c$ (the states of the effort weighting system, $\mathbf{x}_k^f$, could be predicted without error from the actuator signal). The process noise (v_k in Eq. 2) and measurement noise were both assumed to be Gaussian and independent. As shown in Eq. 2, the process noise was assumed to enter the plant through the same path as the control actuator. The ratio of variances of the process and measurement noises is usually unknown and is another design parameter in the control law. This ratio and the shaping of the frequency-dependent control effort weighting have a significant effect on the bandwidth of the controller.

These parameters are compared graphically in Fig. 3. The solid line in Fig. 3(a) shows the magnitude of the frequency response between the synthetic jet actuator and a pressure sensor in the cavity at low Mach number. The dashed line in the plot is the magnitude of a bandstop filter used to penalize control effort. At low and high frequencies the control effort term is greater than the performance curve, hence the control effort term dominates the cost function. The corresponding optimum controller will have low gain in these frequency ranges. Within the stopband of the effort penalty, the sensor response curve dominates, so the controller will have high gain in this area. The floor of the stopband filter is determined by the parameter r in Eq. 4.

For the Kalman estimator, Fig. 3(b) illustrates the relationship between measurement and process noise. Process noise is assumed to enter the plant coincident with the actuator,

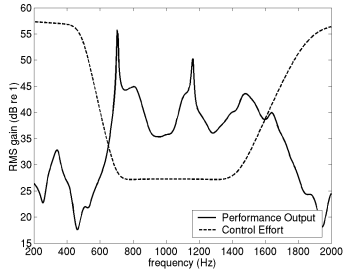

a) Performance vs. Control Effort

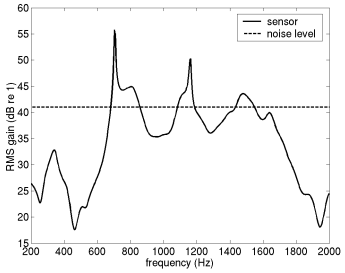

b) Process vs. Measurement Noise

Figure 3: Graphical comparison of control design parameters

hence the figure shows the same transfer function as in Fig. 3(a). Here, the dashed line represents the ratio of the variances of measurement noise to process noise. Only near peaks at 700, 1200, and 1500 *Hz* is the sensor response assumed to be due to the plant model. The Kalman estimator corresponding to this example would be of low gain where measurement noise dominates the sensor response. As a result, the state estimates in these frequency ranges would tend to zero, which has the effect of rolling off the gain of the controller.

Using the notation from Fig. 2, where $G(z)$ denotes the discrete time transfer function from actuator input to sensor responses, and $H(z)$ denotes the transfer function of the feedback controller, the transfer function of closed loop system can be written

$$\frac{Y(z)}{U(z)} = \frac{G(z)}{1 + G(z)H(z)} \tag{6}$$

This equation provides one way to check the stability and performance of the closed loop system. It will also provide some insight into the closed loop performance, but this is of limited utility without complete knowledge of the disturbance spectrum and disturbance path. Errors in the state space model of the plant will also limit the usefulness of Eq. 6 for predicting the actual performance of the controller.

The sensitivity of the closed loop control system is also a useful analysis tool, since it quantifies how sensor noise is amplified or attenuated by the feedback control system.[18] The sensitivity, written as a transfer function of sensor response, $Y(z)$, for a given random noise input, $N(z)$, to the sensor is given by

$$\frac{Y(z)}{N(z)} = \frac{1}{1 + G(z)H(z)} \tag{7}$$

When disturbance rejection is the primary concern, as for the cavity problem, the sensitivity should be small in frequency ranges where the disturbance is to be minimized.

Experimental Setup

The wind tunnel facility, cavity model, and transducers used to implement feedback control are described in this section.

Wind Tunnel Facility

The experiments were conducted in the NASA Langley Probe Calibration Tunnel (PCT). The PCT is typically operated as an open-jet pressure tunnel with independent control of stagnation pressure, stagnation temperature, and free stream velocity. The stagnation pressure and temperature ranges for the facility are 13.8 kPa to 1034 kPa and 255 K to 367 K, respectively. For the current experiments, the facility was fitted with a subsonic nozzle that contracts from a circular inlet to a 50.8 mm by 152.4 mm exit. A straight duct section of length 0.6 m was attached to the nozzle exit and was terminated with a small-angle diffuser. The free stream Mach number range for the present tunnel configuration was 0.04 to 0.8.

Cavity Model

A rectangular cavity model was installed in the ceiling of the straight duct section of the PCT. The floor of the duct section was a foam filled baffle which minimized reflections of acoustic waves radiated by the cavity. The cavity model had a fixed length, $\ell = 152.4$ mm, and a variable depth, d which was fixed to 30.48 mm, for an ℓ/d ratio of 5. The cavity model spanned the width of the test section ($w = 50.8$ mm) to provide an un-obscured view of the cavity shear layer for optical diagnostics. A schematic of the cavity (drawn inverted from its installed position for clarity) is shown in Fig. 1, with actuator and sensor locations indicated.

Sensors

The cavity model was instrumented with a pair of piezoresistive pressure transducers (Endevco model 8510B-2). The sensors had a nominal sensitivity and bandwidth of 2.2×10^{-5} V/Pa and 14 kHz, respectively. One sensor was located in the floor midplane, 18 mm downstream from the cavity front wall. The second sensor was located in the midplane of the rear cavity wall, 19 mm from the cavity trailing edge. The signals from the sensors were pre-amplified and low-pass filtered with 6th order elliptic filters with a corner frequency of 3 kHz. Because these filters are present during system identification, their effect is implicitly accounted for in the plant model.

Different gains were applied to the front and rear sensor responses so the voltages going to the analog to digital converters used as much of the working range of the converters as possible. The system identification model and feedback control system were implemented

in terms of volts of sensor response and volts of actuator input. This means that the two sensors appeared nearly as energetic as one another to the control system, even though in terms of calibrated units the frequency response at the rear sensor was nearly 10 dB higher across the bandwidth than at the front sensor. This result has implications for the sensor weighting matrix, $\mathbf{Q}$, in the control performance function. Specifically, if $\mathbf{Q} = q\mathbf{I}$, where q is a scalar, the controller penalizes both sensor responses equally.

Actuator

It is important to minimize or eliminate disturbances which are fed into the shear layer at the cavity leading edge by acoustic feedback. The point at which actuation is applied is critical; actuation at the cavity leading edge, where the shear layer is most sensitive, should minimize the required control effort. Recent attempts at cavity control have adopted this approach for actuation.[8,12,14]

A piezo-driven synthetic jet was chosen as the actuator for the current study. The exit of the synthetic jet actuator was a rectangular slot, 44.5 *mm* long by 0.5 *mm* high, located just below the cavity leading edge.

Benchtop measurements of the actuator output velocity in a quiescent medium revealed the peak velocity at the slot exit was ≥ 15 *m/sec* over a frequency range of 600 to 1500 *Hz*. However, the slot exit boundary conditions undoubtedly change when placed in the cavity environment, which is expected to cause the magnitude of the exit velocity to change. No attempt was made to characterize the output velocity of the actuator while operating in the cavity environment with flow. The control signal sent to the actuator was not filtered since the actuator's response naturally rolled off above 3 *kHz*.

Control Hardware

The feedback controllers were implemented on a floating point digital signal processor (DSP). The DSP was also used to collect input-output data for system identification. This ensured an accurate measurement of all gains and delays in the control path. The sample rate for all control designs discussed here was 7500 *Hz*.

Results and Discussion

Closed loop performance data was collected over a four day period for over 260 control designs. Variations in model order (the size of the identified state space model of the cavity dynamics), control order (the model order after internal balancing and state reduction), control bandwidth, and sensor noise variance in the state estimator were tested. The results presented here were selected to validate the combined experimental system identification and optimal control design procedure.

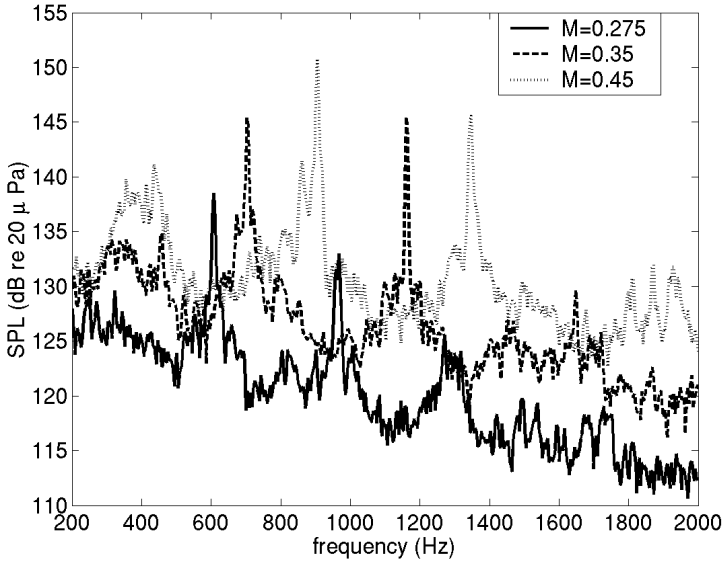

Figure 4: Response of rear pressure transducer at three flow speeds.

In all cases, the cavity was modeled as a single input, two output system, where the input corresponded to the synthetic jet actuator and the outputs to the two pressure sensors in the cavity. All control designs considered both sensors to be equally important in the control cost function. With this assumption, $\mathbf{Q} = q\mathbf{I}$ in Eq. 4, where q is a scalar. Likewise, the sensor noise, $\mathbf{w}_k$ in Eq. 1, was assumed to consist of two independent, white noise signals with equal variance. A fourth order Chebyshev filter was used to implement the bandpass filter for the frequency dependent effort penalty.

This section begins by showing the response of the rear pressure transducer at the three flow speeds of interest. Next, models of the identified transfer function from synthetic jet input to sensor response are described. This is followed by examples of closed loop results at each flow speed. The section ends with a discussion of results from Mach 0.35 which illustrate the complexity of the cavity tone problem.

Open Loop Response

Autospectra of the rear pressure transducer response at flow speeds of Mach 0.275, 0.35, and 0.45, are shown in Fig. 4. The autospectra were computed from 5.3 sec of data with a frequency spacing of 3.7 *Hz*. A Hanning window was applied to the data to reduce leakage. The curves show increasing broadband sound levels with increasing flow speed, and the presence of at least two significant tones at each flow speed. The basic flow physics of these tones were first described by Rossiter,[23] hence the tones are commonly referred to as the Rossiter modes or Rossiter tones of the cavity.

The frequencies of the tones in Fig. 4 agree closely with frequencies predicted by a modified Rossiter equation.[24] The dominant tones in the figure at each flow speed correspond to the second and third Rossiter modes. Table 1 compares measured and predicted frequencies for these tones, using the modified Rossiter equation,[24] where κ was assumed to be 0.66 times the freestream velocity, and α was assumed to be 0.25. These values were empirically determined from experimental data, and are close to values reported in the literature.[24]

Table 1: Measured vs. predicted frequencies (Hz) of the 2nd and 3rd Rossiter modes

Mach	Mode 2		Mode 3	
#	Meas.	Pred.	Meas.	Pred.
0.275	609	604	965	950
0.35	704	737	1160	1159
0.45	903	898	1343	1411

Open Loop Transfer Function

The control methodology assumed that an accurate state space model of the transfer function from actuator input to sensor outputs was available. This model was computed from measured input-output data obtained when the actuator was driven with a random signal with a bandwidth of 100-3700 *Hz*. Due to significant broadband pressure fluctuations from the impinging shear layer and limited actuator authority, the coherence from driving signal to sensor response was low. At all three flow speeds the coherence was less than 0.05 below 500 Hz and above 3 kHz, where the synthetic jet had little control authority. In between those frequencies, the coherence went down with flow speed: < 0.5 at Mach 0.275, < 0.4 at Mach 0.35, and < 0.2 at Mach 0.45. To compensate for the low coherence, long time records (10 seconds) were collected for system identification.

Frequency responses of state space models of actuator input to sensor responses at three flow speeds are shown in Fig. 5. Figure 5(a) shows the magnitude of the frequency response at the pressure sensor in the rear of the cavity, and Fig. 5(b) shows the front sensor. The frequency responses are in terms of volts of sensor response per volt of actuator input, which corresponds to the units used by the control system. In calibrated units, the frequency response to the front sensor was about 10 dB lower than the rear sensor at all frequencies. Because of the very low coherence between actuator input and sensor response, the models should be considered accurate only between about 500 Hz and 1800 Hz. The frequency dependent control effort penalty discussed earlier was used to limit control energy to this middle frequency range. The number of states in each model, listed in the figure legend, was selected so the model's frequency response matched the measured frequency response in this

a) Rear pressure transducer **b)** Front pressure transducer

Figure 5: Modeled frequency response magnitudes at three flow speeds

middle frequency range.

The curves in Fig. 5 offer some insight into the synthetic jet's capabilities as a broadband actuator. At Mach 0.35 and 0.45, the transfer function has high gain near the Rossiter modes, but drops off by 20 dB or more away from the modes. In contrast, at Mach 0.275, peaks near the Rossiter modes are not as distinct, and the transfer function has many small peaks from 600 to 1300 *Hz*. In particular, the transfer function at Mach 0.275 peaks at 800 *Hz*, a frequency which is between Rossiter modes at 609 and 965 *Hz*. A peak at 800 *Hz* is visible to some degree at all three flow speeds, and is probably due to a resonance of the piezoelectric actuator in the synthetic jet. At all three flow speeds the transfer function gain rolls off at high and low frequencies.

Identified state space models of the actuator to sensor dynamics appeared to remain accurate over a few hours of testing at a given flow speed. For a given flow condition, a state space model was computed from input-output data and then used to generate a suite of different control designs. These control designs might include variations of sensor noise variance, control bandwidth, and control order. The control designs were then individually tested with the tunnel at the same flow condition. In some cases, a few hours elapsed between the collection of system identification data and the evaluation of a control design. However, the results did not indicate that closed loop performance depended on the elapsed time since system identification was collected. This suggests that both the tunnel conditions and the dynamics of the tone generation mechanism did not change significantly over a few hour period.

Closed Loop Results

Results obtained using the best control designs at the three flow speeds are presented in this section. The results are quantified by comparing open and closed loop autospectra of the rear sensor response. For these cases, similar reductions were obtained at the front and

rear sensors, but only the rear sensor response is discussed for simplicity.

Figures 6(a), 6(c), and 6(e) show the pressure measured at the rear sensor for open loop (*No Control*) and closed loop (*Control*) cases at the three flow speeds. The closed loop results show the controller was able to reduce multiple tones at each flow speed, and a slight reduction in the broadband level was obtained at the two higher flow speeds.

At Mach 0.275, the three most prominent tones in the spectrum, corresponding to the 2nd, 3rd, and 4th Rossiter modes, were reduced by 7.8 dB, 6.9 dB, and 4.1 dB, respectively. However, the controller excited a new tone above the 4th mode at 1550 *Hz*. At Mach 0.35 the 2nd and 3rd Rossiter modes were reduced by 7.9 dB and 10.1 dB, respectively. The sidebands near the 3rd mode at 1160 *Hz* were increased by the controller. A slight reduction in the broadband level is apparent between the two tones. The peak in the open loop response at 460 *Hz* was caused by a difference interaction due to quadratic coupling between the two Rossiter modes. As the peak levels of those two tones dropped, the peak level of the 460 *Hz* tone also dropped. Smaller reductions were obtained at Mach 0.45, where the 2nd Rossiter mode was reduced by 5.0 dB and the 3rd mode was reduced by 6.5 dB. A slight reduction in the broadband level is evident between the two tones.

The control and estimator design parameters for these three cases are listed in Table 2. The first column lists the run number. The number of states for the full state space model identified from the input-output data are listed next, followed by the order of the reduced state space model, from which the controller was designed. Columns 5-8 list the properties of the bandstop filter used to penalize control effort. The stopband and passband levels are listed in units of dB of transfer function gain, corresponding to the transfer functions shown in Fig. 5. These units make it easier to compare the effort penalty filter to the transfer function gain, as in the discussion of Fig. 3(a). The sensor noise variance used to compute the state estimator, listed in the last column of the table, is also expressed in units of transfer function gain.

Table 2: Control design parameters

Run #	Mach #	# of states		Effort penalty parameters				Sensor Noise (dB)
		Full model	Reduced model	f_{min} (Hz)	f_{max} (Hz)	stopband gain (dB)	passband gain (dB)	
1355	0.275	199	80	500	1600	1	51	31
1428	0.35	160	60	400	1700	23	57	43
1535	0.45	195	60	400	2000	31	61	44
1418	0.35	160	60	300	2500	17	57	43

Open and closed loop transfer functions from the actuator input to the rear sensor are

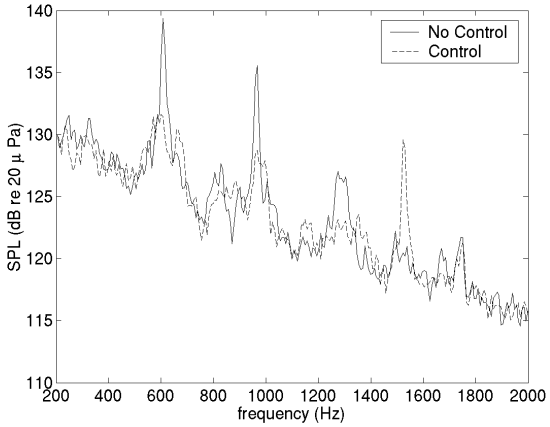

a) Mach 0.275 (Run 1355): Rear sensor response with and without control.

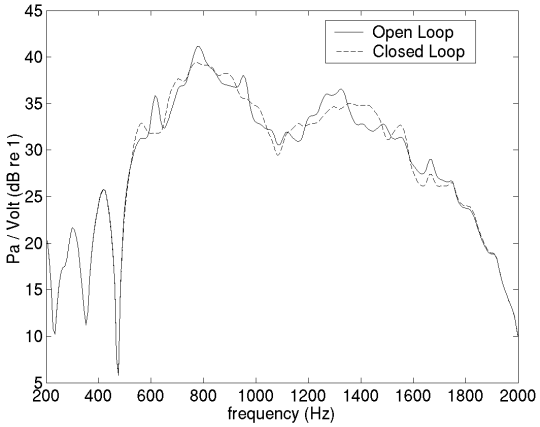

b) Mach 0.275 (Run 1355): Open and closed loop transfer function from actuator to rear sensor.

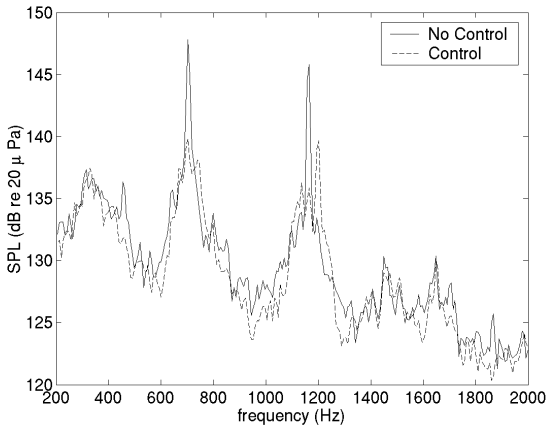

c) Mach 0.35 (Run 1428): Rear sensor response with and without control.

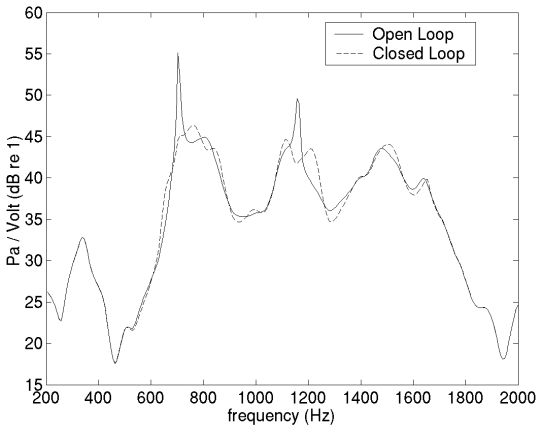

d) Mach 0.35 (Run 1428): Open and closed loop transfer function from actuator to rear sensor.

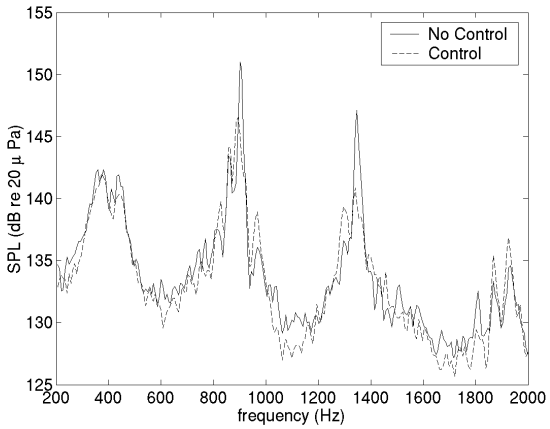

e) Mach 0.45 (Run 1535): Rear sensor response with and without control.

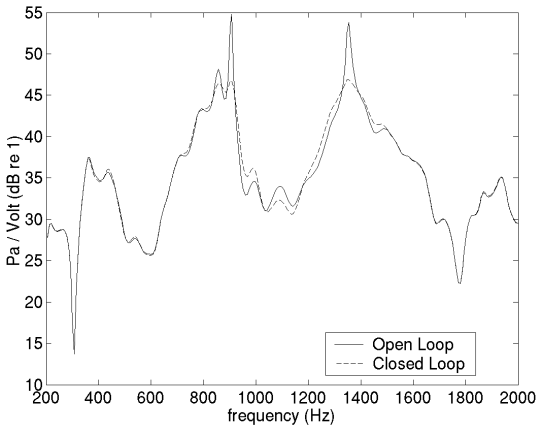

f) Mach 0.45 (Run 1535): Open and closed loop transfer function from actuator to rear sensor.

Figure 6: Measured and modeled control performance at three flow speeds

shown in Figs. 6(b), 6(d), and 6(f). The solid curve shows the open loop transfer function, $G(z)$, while the dashed curve shows the closed loop transfer function computed using Eq. 6. In each case a state space model, such as one of those shown in Fig. 5, was used for the open loop transfer function. These curves can't be directly compared with the measured data since the measured results correspond to a different transfer function driven by an unknown disturbance. Nonetheless, if trends in the closed loop model match trends in the measured results, it would validate the state space model and thereby validate the assumption of linearity. It is also useful to know if the closed loop transfer function can be used to optimize the control design, without having to close the loop and collect data on every design.

At all three flow speeds the closed loop model shows varying amounts of disturbance attenuation and amplification in different frequency ranges. Specifically, the model shows disturbance attenuation whenever the dashed line is less than the solid line. At Mach 0.275, Figure 6(b) indicates the controller will attenuate the disturbance near the Rossiter modes at 610, 960, and 1250 *Hz*, which agrees with the measured results. The closed loop model also shows disturbance amplification above 610 *Hz*, below 1200 *Hz*, and near 1550 *Hz*. The measured results verify that with control on, the sensor response increased at these frequencies. The magnitude of disturbance amplification seen in the measured results near 1550 *Hz* is curious, since the prediction doesn't suggest such a large amplification. Assuming a linear system and a constant disturbance, the tone at 1550 *Hz* could be due to an error in the state space model.

Trends in the open and closed loop transfer functions in Figs. 6(d) and 6(f) also agree with measured results. At Mach 0.35, Fig. 6(d) shows a slight amplification of the disturbance just above the cavity tone at 700 *Hz*, and the measured results agree. Amplification is also predicted and was measured above and below the mode at 1160 *Hz*. The measured reduction at 460 *Hz* was not predicted by the linear model, which is to be expected since this tone was due to a non-linear effect.

Control spillover and non-linear dynamics

In addition to demonstrating reductions of multiple cavity tones, the preceding results also show spillover of control energy. For example, Fig. 6(a) shows a peak created by the control system near 1550 Hz, and Fig. 6(c) shows spillover just above the cavity tone near 1200 Hz. Some of this spillover of energy can be explained by looking at the gain and phase of the closed loop system, using the expression given in Eq. 6. For example, the magnitudes of the closed loop transfer functions in Figs. 6(b), 6(d), and 6(f) all show some disturbance amplification in the sidebands of the cavity tones. This can be attributed to two factors: the large control gain concentrated in a narrow frequency band about the cavity tones, and the

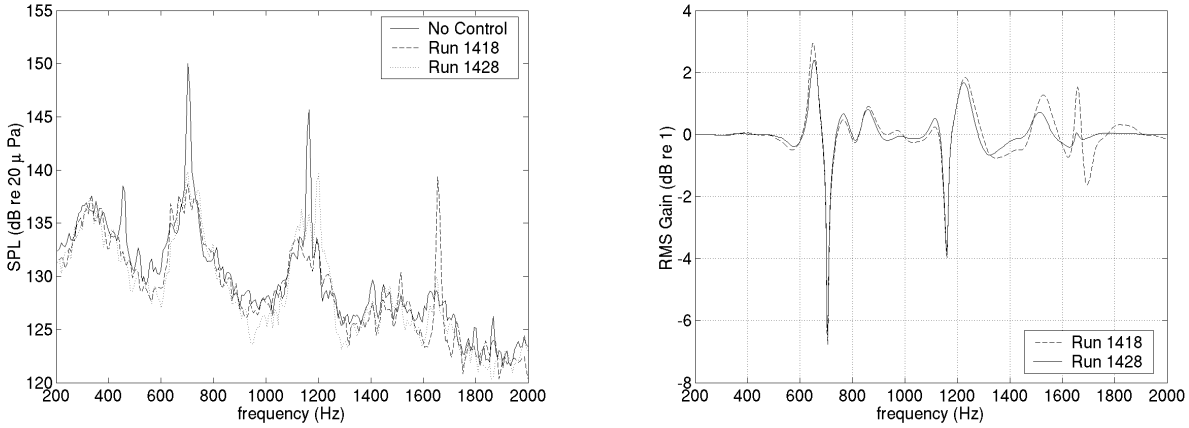

a) Measured performance, M=0.35. **b)** Sensitivity, M=0.35.

Figure 7: Control performance at Mach 0.35 and sensitivity

significant time delay from actuator input to sensor response. Previous works have discussed this tendency in greater detail, in the context of the cavity tone problem and for controlling combustion instabilities.[10,25,26]

Notwithstanding the agreement between the modeled and measured results, there are non-linearities in the cavity problem which deserve consideration. To illustrate, results from a second control design at Mach 0.35, labeled Run 1418, are shown in Fig. 7(a) with results from Run 1428 discussed previously. The Run 1418 controller reduced the two Rossiter modes without increasing the sidebands, but it generated a secondary tone at 1660 Hz. Instead of comparing the closed loop transfer functions for these two controllers, it is easier to compare the magnitude of the sensitivity (Eq. 7), shown in Fig. 7(b). The sensitivity for Run 1418 shows disturbance amplification at 1650 Hz, which corresponds to the secondary tone found in the measured results. Disturbance amplification of nearly the same level is also predicted near 1500 Hz for Run 1418, but the measured results show very little amplification there. Near the third Rossiter mode at 1160 Hz, the sensitivity for the controllers is similar to one another, although the magnitude for Run 1418 is slightly higher than Run 1428 at 1200 Hz. This data suggests that Run 1418 should excite the upper sideband of the third Rossiter mode at least as much as Run 1428, but the measured results show this wasn't true.

It is not known exactly why the sideband excitation of the two controllers was so different, but it may have been due to mode competition, where forced and natural frequencies compete for available energy in the shear layer. This competition between frequencies has been leveraged before in open and closed loop control configurations,[6,9] where the shear layer is driven with a secondary frequency in order to inhibit the natural feedback loop in the cavity. This non-linear interaction between frequencies will obviously not be predicted by linear

models.

Results similar to those shown in Fig. 7 were observed in numerous closed loop control cases. Specifically, the closed loop performance of many controllers was limited by excitation of the sidebands of a Rossiter mode. Aggressive controllers which didn't excite the sidebands tended to create a secondary tone, like Run 1418. Some possible causes for this behavior are: inaccuracies in the identified plant model; side effects of high gain controllers and time delays in the plant; or, changes in the dynamics of the system once control is applied. A combination of these factors is also possible. Unfortunately, the current set of measurements is not sufficient to determine the cause for the limitations in controller performance.

Conclusions

Discrete-time linear quadratic control design methods using state space models computed from experimental data were successfully applied to the cavity tone problem. The controller consisted of a synthetic jet actuator at the leading edge of the cavity and two pressure transducers mounted inside the cavity. At Mach 0.275, the 2nd, 3rd, and 4th Rossiter modes were reduced by 7.8 dB, 6.9 dB, and 4.1 dB. At Mach 0.35, the 2nd and 3rd Rossiter modes were reduced by 7.9 dB and 10.1 dB, while at Mach 0.45, the 2nd and 3rd modes were reduced by 5 and 6.5 dB, respectively. With the exception of the 3rd mode at Mach 0.35, the tonal levels were reduced without exciting sidebands of the tones. At Mach 0.275, the controller excited an extraneous tone that was 200 Hz above the 4th Rossiter mode. General trends of disturbance amplification and attenuation found in the measured results agreed with predictions based on linear models.

Although linear models of the cavity and closed loop system generally agreed with measured results, the models do have limitations. For example, a linear model was shown to inadequately account for a strong tone at a high frequency affecting the dynamics at a lower frequency. Additional measurements are needed to better quantify the dynamics from actuator to sensor in the cavity.

References

[1]Kibens, V. and Bower, W. W., "An Overview of Active Flow Control Applications at The Boeing Company," *2nd AIAA Flow Control Conference*, No. AIAA-2004-2624, Portland, OR, June 2004.

[2]Tilmann, C. P., Kimmel, R. L., Addington, G. A., and Myatt, J. H., "Flow Control Research and Applications at the AFRL's Air Vehicles Directorate," *2nd AIAA Flow Control Conference*, No. AIAA-2004-2622, Portland, OR, June 2004.

[3]Shaw, L., Bartel, H., and McAvoy, J., "Acoustic Environment in Large Enclosures With a Small Opening Exposed to Flow," *Journal of Aircraft*, Vol. 20, No. 3, 1983, pp. 250–256.

[4]Cain, A., Rubio, A., Bortz, D., Banks, H., and Smith, R., "Optimizing Control of Open Bay Acoustics," *6th AIAA/CEAS Aeroacoustics Conference*, No. AIAA-2000-1928, Lahaina, HI, June 2000.

[5]Shaw, L. and Northcraft, S., "Closed Loop Active control for cavity acoustics," *33rd AIAA Thermophysics Conference*, No. AIAA-99-1902, Norfolk, VA, June 1999.

[6]Shaw, L., "High Speed Application of Active Flow Control for Cavity Acoustics," *6th AIAA/CEAS Aeroacoustics Conference*, No. AIAA-2000-1926, Lahaina, HI, June 2000.

[7]Mendoza, J. and Ahuja, K., "Cavity Noise Control Through Upstream Mass Injection from a Coanda Surface," *2nd AIAA/CEAS Aeroacoustics Conference*, No. AIAA-96-1767, State College,PA, May 1996.

[8]Williams, D. R., Fabris, D., and Morrow, J., "Experiments on controlling multiple acoustic modes in cavities," *6th AIAA/CEAS Aeroacoustics Conference*, No. AIAA-2000-1903, Lahaina, HI, June 2000.

[9]Cattafesta III, L., Garg, S., Choudhari, M., and Li, F., "Active Control of Flow-Induced Cavity Resonance," *28th AIAA Fluid Dynamics Conference*, No. AIAA-97-1804, Snowmass Village, CO, June 1997.

[10]Rowley, C., Williams, D., Colonius, T., Murray, R., MacMartin, D., and Fabris, D., "Model-Based Control of Cavity Oscillations Part II: System Identification and Analysis," *40th AIAA Aerospace Sciences Meeting and Exhibit*, No. AIAA-2002-0972, Reno, NV, Jan. 2002.

[11]Huang, X. and Weaver, D., "On the Active Control of Shear Layer Oscillations Across a Cavity in the Presence of Pipeline Acoustic Resonance," *Journal of Fluids and Structures*, Vol. 5, 1991, pp. 207–219.

[12]Williams, D. R. and Morrow, J., "Adaptive Control of Multiple Acoustic Modes in Cavities," *31st AIAA Fluid Dynamics Conference*, No. AIAA-2001-2769, Anaheim, CA, June 2001.

[13]Williams, D., Rowley, C., Colonius, T., Murray, R., MacMartin, D., Fabris, D., and Albertson, J., "Model-Based Control of Cavity Oscillations Part I: Experiments," *40th AIAA Aerospace Sciences Meeting and Exhibit*, No. AIAA-2002-0971, Reno, NV, Jan. 2002.

[14]Cattafesta, L., Shukla, D., Garg, S., and Ross, J., "Development of an adaptive weapons-bay suppression system," *33rd AIAA Thermophysics Conference*, No. AIAA-99-1901, Norfolk, VA, May 1999.

[15]Venugopal, R. and Bernstein, D. S., "Adaptive Disturbance Rejection Using ARMARKOV/Toeplitz Models," *IEEE Transactions on Control Systems Technology*, Vol. 8, No. 2, March 2000, pp. 257–269.

[16]King, R., Becker, R., Garwon, M., and Henning, L., "Robust and adaptive closed-loop control of separated shear flows," *2nd AIAA Flow Control Conference*, No. AIAA-2004-2519, Portland, OR, June 2004.

[17]Cattafesta III, L. and Garg, S., *Active Suppression of Shear-Layer/Cavity Resonance Interactions, Final Technical Report, Contract NAS2-14248*, NASA Ames Research Center, 1997.

[18]Anderson, B. and Moore, J., *Optimal Control - Linear Quadratic Methods*, Information and System Sciences Series, Prentice Hall, Englewood Cliffs, New Jersey, 1990.

[19]Mosca, E., *Optimal, Predictive, and Adaptive Control*, Prentice Hall, 1995.

[20]Juang, J.-N., *Applied System Identification*, Prentice Hall, 1994.

[21]Juang, J.-N., "State-Space System Realization with Input and Output Data Correlation," Tech. Rep. TP-3622, NASA Langley Research Center, April 1997.

[22]Gibbs, G. P., Eure, K. W., and Lloyd, J. W., "Active Control of Turbulent Boundary Layer Induced Sound Radiation from Aircraft Style Panels," *Proceedings of Active-99*, Ft. Lauderdale, Florida, Dec. 1999.

[23]Rossiter, J., *Wind-Tunnel experiments on the flow over rectangular cavities at subsonic and transonic speeds*, Aeronautical Research Council Reports and Memoranda No. 3438, Oct. 1964.

[24]Heller, H., Holmes, D., and Covert, E., "Flow-induced pressure oscillations in shallow cavities," Tech. Rep. TR-70-104, AFFDL, Dec. 1970.

[25]Banaszuk, A., Jacobsen, C. A., Khibnik, A. I., and Mehta, P. G., "Linear and Nonlinear Analysis of Controlled Combustion Processes. Part I: Linear Analysis," *Proceedings of the 1999 IEEE International Conference on Control Applications*, Kohala, Hawai'i, Aug. 1999, pp. 199–205.

[26]Saunders, W., Vaudrey, M., Eisenhower, B., Vandsburger, U., and Fannin, C., "Perspectives on Linear Compensator Designs for Active Combustion Control," *37th AIAA Aerospace Sciences Meeting and Exhibit*, No. AIAA-1999-0717, Reno, NV, Jan. 1999.